arXiv:cond-mat/0310437v1 18 Oct 2003

Variational Monte Carlo study of the ground state properties and vacancy formation energy of solid para-H_2 using a shadow wave function

Francesco Operetto

Dipartimento di Fisica, Università di Trento,

via Sommarive, 14 I-38050 Povo, Trento, Italy

Francesco Pederiva

Dipartimento di Fisica, Università di Trento,

via Sommarive, 14 I-38050 Povo, Trento, Italy and

INFM DEMOCRITOS National Simulation Center, Trieste, Italy

(Dated: March 22, 2022)

Abstract

A Shadow Wave Function (SWF) is employed along with Variational Monte Carlo techniques to describe the ground state properties of solid molecular para-hydrogen. The study has been extended to densities below the equilibrium value, to obtain a parameterization of the SWF useful for the description of inhomogeneous phases. We also present an estimate of the vacancy formation energy as a function of the density, and discuss the importance of relaxation effects near the vacant site.

PACS numbers: 67.80.Mg,05.30.Jp

I. INTRODUCTION

The properties of molecular para-hydrogen (p-H_2) have been the subject of intense experimental and theoretical investigation over the years. One main research direction is related to the existence of a metallic phase at very large pressures[1, 2, 3, 4, 5, 6, 7]. On the other hand, the Bosonic nature and the very small mass of p-H_2 would naturally lead to the search for the existence of a superfluid phase. The strong H_2–H_2 interaction, however, causes the zero–pressure ground state of p-H_2 to be a crystal at T=0. The only possibility of finding p-H_2 in a fluid phase at temperatures lower than 6K[8], where a superfluid transition is believed to occur, comes from geometry–constrained or strongly inhomogeneous systems.

It has been shown by Sinzingdre et al.[9] using Path–Integral Monte Carlo methods that small p-H_2 clusters with a number of molecules N$\leq$13 preserve a liquid character, and show the signatures of superfluidity. Recently Levi and Mazzarello[10] proposed that the existence of such liquid clusters might depend on the difficulty for the system to go over the nucleation energy barrier in a time comparable to the lifetime of the clusters themselves. The determination of such energy barrier depends on the knowledge of a number of physical parameters, but in particular on the solid–liquid interface energy. It was recently shown that superfluid p-H_2 could also be found in two dimensional layers deposited on substrates such as graphite. Recent PIMC calculations showed that at full coverage the density of a monolayer is too large for allowing the system to have a stable liquid phase. However, the presence of alkali impurities, that exert a very weak attraction on the hydrogen molecules, can stabilize a disordered phase reducing the strong p-H_2 -p-H_2 interaction[11, 12]. The same effect can be studied reducing the coverage and looking at two–dimensional p-H_2 clusters at the surface. If the number of atoms in a single cluster is small enough (N $\leq$ 30) the stable configuration is a puddle of liquid[13]. The occurrence of surface melting at the surface of a thick (5 to 7 monolayers) layer of p-H_2 was also studied by PIMC techniques for temperatures $>$ 3K[14].

Recent experiments performed by Grebenev et al.[15] on a OCS–p-H_2 immersed in ^{4}He and mixed ^{4}He–^{3}He clusters clearly show that the hydrogen coating the molecule undergoes a transition at a temperature between 0.38K and 0.15K. This transition can be inferred by the change in the measured rotational spectrum, and therefore of the momentum of inertia, when the OCS–p-H_2 complex is included in a pure ^{4}He cluster and when also ^{3}He is present. Recent simulation work confirms the occurrence of this transition[16].

From the theoretical point of view the simulation approach is the most effective in studying inhomogeneous phases. In this paper we extend to the study of p-H_2 a technique that revealed extremely powerful in the description of inhomogeneous phases of ^{4}He with large numbers of particles: Variational Monte Carlo calculations based on Shadow Wave functions (SWF)[17, 18]. The main property of SWF is the capability of describing the crystalline and the disordered phase of a quantum system with the same translationally invariant form. It was therefore possible to study coexisting liquid–solid[19] and liquid–vapor[20] systems in ^{4}He as well as finite systems like ^{4}He clusters with and without impurities[21]. This method, although not exact, gives quantitatively significant results, as for instance a realistic estimate of the interface energy of solid ^{4}He[19], in situations where other techniques, like Path Integral MC or Diffusion MC, are harder to apply. Some early calculations using SWF for small p-H_2 clusters (N$\leq$7) were performed by Rama Krishna and Whaley[22]. However, their form of the wave function used cannot be immediately extended to bulk systems. In this paper we introduce a SWF optimized and parametrized in a form directly usable in calculations where the parameters become functions of the *local* density of the system[19]. With this wave function, we carried out a systematic study of the ground state properties of the bulk solid at densities up to 1.6 times the equilibrium density, and also to metastable bulk states below the equilibrium, beyond the limit of stability of the ordered phase. We also present results for an estimate of the vacancy formation energy in p-H_2 as a function of the crystal density.

II. METHODS

A. Hamiltonian

Molecular para-hydrogen is here described as a collection of N point-like particles interacting via a two-body potential:

$$\hat{H} = -\frac{\hbar}{2m}\sum_{i=1}^{N} + \sum_{i<j} v(r_{ij}). \tag{1}$$

The model potential we chose is the Silvera-Goldman (SG)[23] potential, which takes the form:

$$v(r) = A[v_{rep} + (v_{att} + v_{dd}) f_c(r)], \tag{2}$$

r_m (Å)	3.41
D	1.28
a	10.923340
b	10.098343
γ	0.4122340
C_6	1.69550147
C_8	0.71379389
C_9	0.07468938
C_{10}	0.38990868
A (K)	31.5763295

TABLE I: Parameters of the SG potential[23]. All parameters are non–dimensional, except for r_m, which is given in Å, and A, which is given in K

where, using $\tilde{r} = r/r_m$.

$$
\begin{aligned}
v_{rep}(r) &= \exp(a - b\tilde{r} - \gamma\tilde{r}^2) \\
v_{att}(r) &= -\left(\frac{C_6}{\tilde{r}^6} + \frac{C_8}{\tilde{r}^8} + \frac{C_{10}}{\tilde{r}^{10}}\right) \\
v_{dd}(r) &= \frac{C_9}{\tilde{r}^9} \\
f_c(r) &= \begin{cases} \exp\left[-\left(\frac{D}{\tilde{r}} - 1\right)^2\right] & \text{if } r < D\, r_m \\ \\ 1.0 \text{ if } r > D\, r_m \end{cases} .
\end{aligned}
\tag{3}
$$

The values of the parameters are given in table I.

The $C_9/\tilde{r}^9$ term is introduced as an effective many–body force, assuming that the leading term is a triple-dipole contribution, which is usually introduced as a three-body Axilrod-Teller force. However, this parameterization is effective for studying isotropic properties of the system, and the replacement of the three-body term with a pair term is a second order effect. Variational Monte Carlo calculations by Norman et al.[24], using a Bijl-Jastrow-Nosanow [25] trial wave function, show that within this model the GS potential is in qualitative agreement with experiments in a wide range of densities; other model interactions (like the Schaefer-Watts potential[26] or the Buck et al. potential[27]) give better values

around the equilibrium density, but become worse at higher pressure.

B. Shadow Wave Function

We use as trial solution for the N-molecules Hamiltonian at T=0K a Shadow Wave Function[17, 18], having the following general form:

$$\Psi(R) = \int K(R,S)\phi(S)\, dS, \tag{4}$$

where $R = \{\mathbf{r}_1 \dots \mathbf{r}_N\}$ and $S = \{\mathbf{s}_1 \dots \mathbf{s}_N\}$ are the molecular and auxiliary ("shadow") degrees of freedom respectively. The kernel K is written as the product of a Jastrow–pair wavefunction involving the molecular degrees of freedom, times a term coupling molecular and shadow positions:

$$K(R,S) = \prod_{i<j} \exp\left[-\frac{1}{2}\left(\frac{b}{r_{ij}}\right)^5\right] \prod_{i=1}^{N} \exp\left[-C\left(\mathbf{r}_i - \mathbf{s}_i\right)^2\right] \tag{5}$$

The shadow degrees of freedom are also correlated by $\phi(s)$, a Jastrow product of the same form of the one used for the molecules. The correlation pseudopotential is the rescaled intermolecular interaction[28]:

$$\phi(s) = \exp\left[-\delta \sum_{i<j} v(\alpha s_{ij})\right]. \tag{6}$$

The parameters b, C, δ, α appearing in the SWF are determined variationally, by minimizing the variance of the expectation value of the Hamiltonian

$$\langle \Delta E^2 \rangle = \frac{\langle \Psi(R) | (H - E_0)^2 \Psi(R) \rangle}{\langle \Psi(R) | \Psi(R) \rangle}. \tag{7}$$

As already mentioned, SWF provides a stable crystalline phase despite its translationally invariant form, due to the implicitly induced many–body correlations. The stable phase, ordered or disordered, is determined by the variational parameters minimizing the variance of the energy.

For comparison we also performed VMC calculations with a standard Bijl–Jastrow–Nosanow wavefunction[25], in which the atoms are constrained to remain around given lattice positions:

$$\Psi(R) = \exp\left[-\frac{1}{2}\sum_{i<j}\left(\frac{b}{r_{ij}}\right)^5\right] \prod_{i=1}^{N} \exp[-C(\mathbf{r}_i - \bar{\mathbf{R}}_i)^2], \tag{8}$$

where the $\bar{\mathbf{R}}$ are vectors of a lattice. This wave function has been also taken as importance function for the Diffusion Monte Carlo result that we computed at equilibrium density.

C. Simulations

All simulations have been performed for a cell of constant volume V containing a number N of molecules such that $\rho = N/V$, and imposing periodic boundary conditions in order to reduce finite–size effects. The simulations have been performed for two different crystal geometries: face-centered cubic (fcc) and hexagonal close-packed (hcp). Most of the results for the fcc crystal were obtained using N=108 molecules arranged on 3x3x3 elementary cubic cells of side $a_{cell} = (4/\rho)^{\frac{1}{3}}$). For simulations in the hcp phase we considered N=180 molecules in a cell made up of 5x3x3 elementary cells. In order to check the magnitude of finite size effects (in particular for the vacancy formation energy) simulations in the fcc crystal with N=256 (4x4x4 elementary cubic cells) and N=500 (5x5x5 elementary cubic cells) have also been performed.

The molecule-molecule interaction is truncated at the edge of a sphere of radius equal to half of the side of the simulation box L. The contribution from the potential energy outside the sphere is estimated by assuming that the pair correlation function is constant for distances larger than $L/2$.

The expectation values of the observables of interest have been computed by means of the Variational Monte Carlo method. When using SWF, the expectation value of a local operator $\hat{O}(R)$ is given by:

$$\langle \hat{O} \rangle = \frac{1}{\mathcal{N}} \int \int \int \pi(R, S, S') \hat{O}(R) dR \, dS \, dS', \tag{9}$$

where $\mathcal{N}$ is the normalization of the wave function. This integral can be computed sampling the joint probability distribution for the molecular and shadow degrees of freedom:

$$\pi(R, S, S') = K(R, S)\phi(S)K(R, S')\phi(S'). \tag{10}$$

As we illustrated in previous work[29], the use of plain Metropolis sampling considerably slows down the convergence of the results, especially when the crystal includes a vacancy. This is due to the fact that the probability for a particle to have a given displacement is conditional on the position of the corresponding shadow degrees of freedom, to which it

is connected by harmonic-like terms. The structure of the system is therefore analogous to that of a collection of trimers, whose single components can have only limited relative moves. By using pseudoforces (i.e. gradients of the function to be sampled) in sampling the probability distribution π, it is possible to move all the components of a trimer together. This was demonstrated to be a very powerful tool in the study of vacancies in solid ^{4}He, where it was shown that both relaxation of the density around the empty site and a mobility of the vacancy can be achieved[29, 30]. The use of gradients also improves the convergence in the disordered phase, and in metastable crystal phases, where the low density might give rise to local disordering of the system. The optimization of the variational parameters appearing in the SWF was performed using the optimization program by C.J. Umrigar and P. Nightingale implementing a modified Levemberg-Marquardt algorithm. The optimization of the parameters of the shadow–shadow correlation pseudopotential of Eq. (6) is particularly demanding from the computational point of view. In fact the local energy does not depend, configuration by configuration, on the value of δ and α, but on the statistical weight of the configuration $\pi(R, S, S')$ only. The global computational cost of our SWF, including the optimization stage, is comparable with that of a DMC simulation for the same system. However, once a satisfactory parameterization has been obtained, successive simulations have a cost which is at least one order of magnitude less than DMC. For this reason SWF can be used for simulations including up to several thousands particles, as it was done for the study of the solid-liquid coexistence in ^{4}He.

III. RESULTS

A. Parameterization of SWF

The optimized variational parameters in the SWF each have a different density dependence. The density dependence is exploited in the Local-Density dependent version of the SWF (LD-SWF)[19] that is used for describing inhomogeneous systems, like the solid-vapor interface, with a single wavefunction. For such reason the optimization has to be carried out accurately in the region close to the equilibrium density (which is experimentally found at $\rho_0 = 0.02595\text{Å}^{-3}$[2]), and lower. The parameters b, connected to the width of the correlation hole of the molecules, and C, giving the inverse of the mean square displacement between

α_0	1.2049±0.0872
α_1	-21.961±2.984
δ_0	-0.0047±0.0008
δ_1	0.3717±0.0370

TABLE II: Values of the coefficients of Eq. (11) for the fits of the shadow-shadow pseudopotential parameters α and δ as a function of the density.

particles and shadows, show a weak dependence on the density. In particular the parameter C is nearly constant and equal to 1Å^{-2} throughout the density range considered. The parameter b tends to saturate at high densities around a value 3.35Å, while at equilibrium density its value is $b = 3.25$Å. For densities lower than the equilibrium density the parameter b shows some oscillations, contained within 5% of the value at equilibrium value. Such oscillations might be due to the fact that the system and autocorrelations between configurations become very large, making the optimization difficult. For such reasons a reasonable choice in the LD-SWF is to keep the parameters b and C constant at the value optimal at the equilibrium density. The remaining variational parameters α and δ show a stronger density dependence. As already mentioned the energy at a given density has a much weaker dependence on the values of the shadow–shadow correlation parameters, due to the fact that $\phi(S)$ does not enter in the estimate of the local energy. In Fig. 1 we show the results of the optimization. The errorbars indicate the range of values for which the variation in the computed variational energy is within two standard deviations from the optimal value. These parameters need to be made functions of the density in the LD-SWF. It is reasonable to assume a linear dependence of the parameters α and δ on the density

$$\begin{aligned} \alpha(\rho) &= \alpha_0 + \alpha_1 \rho \\ \delta(\rho) &= \delta_0 + \delta_1 \rho. \end{aligned} \tag{11}$$

The coefficients of the linear fits are given in Table II. The interpolations are also plotted in Fig. 1. The differences between energies computed with the optimal values of the parameters and the values for the LD-SWF parameterization less than 1%.

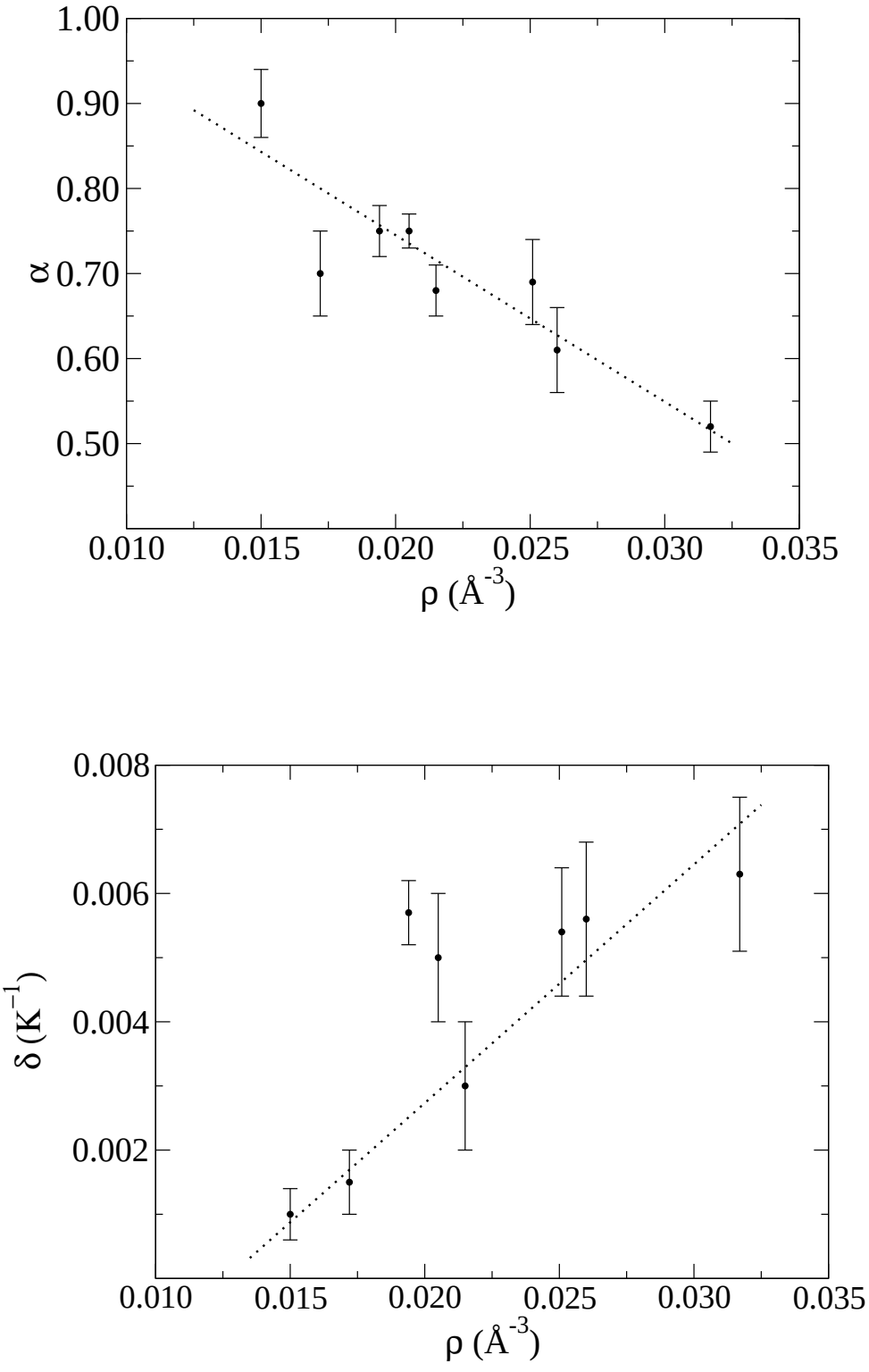


FIG. 1: Dependence of the SWF variational parameters α (upper panel) and δ (lower panel) on the molecular density. Lines show the linear fits to the computed values.

	E/N(K)
SWF	-86.679(3)
JN	-86.214(2)
DMC	-87.931(5)
Exp.	-93.5

TABLE III: Ground state energies per particle at the density $\rho_0 = 0.02609\text{Å}^{-3}$ obtained by VMC with SWF and JN, compared to the DMC result and the experimental value from Ref.24

B. Ground state properties

The SWF has been used to compute the variational energies for molecular p-H_2 . The results are reported in tables III-IV. In table III we compare the binding energy for the density $\rho_0 = 0.02609\text{Å}^-3$, (corresponding to a specific volume $v = 23.08\text{cm}^3$ mol^{-1}) obtained by SWF, variational Monte Carlo with a Jastrow-Nosanow wave function (JN) and Diffusion Monte Carlo (DMC). We also compare to the experimental value reported in Ref. 24 As it can be seen the energy obtained by SWF improve the Jastrow–Nosanow result. Nevertheless the difference between the SWF and DMC results is still larger than 1K. The DMC result at this density shows a quite large discrepancy (about 6%) with respect to the available experimental results. This is in agreement with the findings of Norman et al., who point out that other model interactions give a better estimate of the binding energy near the equilibrium density.

In Table IV we report the variational results obtained with our SWF in the disordered phase and in the crystalline phase, for which values for the fcc and hcp crystals are given. The results are also plotted in Fig. 2. The binding energy for the hcp lattice is lower than for the fcc lattice for densities $\rho < 0.03170\text{Å}^{-3}$.

As already mentioned, when using shadow wavefunctions, the stable phase (crystalline or disordered) is determined entirely from the variational principle. Therefore, given a set of variational parameters, we do not know *a priori* if the molecules will stay localized on a lattice. In order to determine the phase of the system, we need to compute a crystalline

TABLE IV: Total, potential, and kinetic energies per particle, in K, as a function of density from VMC-SWF calculations. For densities at which the system was found to be a crystal, the values are listed for the fcc and hcp lattices (obtained with N=108 and N=180 molecules respectively).

ρ	E_0/N	T/N	V/N			
0.0050	-17.400(16)	4.139(15)	-21.540(10)			
0.0080	-29.348(13)	8.202(16)	-37.476(10)			
0.0110	-41.390(9)	14.269(14)	-55.543(7)			
0.0150	-55.929(5)	24.037(5)	-79.966(3)			
0.0172	-63.800(7)	34.019(9)	-97.713(6)			
		fcc			hcp	
	E_0/N	T/N	V/N	E_0/N	T/N	V/N
0.01940	-70.862(5)	43.469(5)	-114.332(7)	-71.288(6)	43.499(11)	-114.787(11)
0.02150	-79.553(2)	52.029(3)	-131.582(3)	-79.597(6)	52.665(9)	-132.262(7)
0.02509	-86.354(2)	66.541(4)	-152.895(4)	-86.494(4)	66.502(9)	-152.996(8)
0.02600	-86.679(3)	71.400(5)	-158.079(5)	-86.813(5)	71.395(15)	-158.209(15)
0.02900	-83.425(4)	83.868(9)	-167.293(11)	-83.571(7)	83.877(19)	-167.448(21)
0.03170	-73.296(5)	97.142(10)	-170.438(12)	-73.442(9)	97.111(19)	-170.553(23)
0.03400	-58.691(8)	109.237(18)	-167.927(18)	-58.484(3)	109.375(5)	-167.858(5)
0.03700	-30.281(11)	122.924(22)	-153.206(25)	-30.139(2)	122.976(4)	-153.115(5)
0.04000	8.861(2)	141.570(3)	-132.708(4)	8.931(2)	141.450(5)	-132.519(2)

order parameter of this form:

$$O = \frac{1}{NM} \sum_{i=1}^{N} \sum_{\alpha=1}^{M} \left| e^{-i\mathbf{k}_\alpha \cdot \mathbf{r_i}} \right|, \tag{12}$$

where the $\mathbf{k}_\alpha, \alpha = 1...M$ are vectors of the reciprocal lattice for which the order is monitored. This quantity is exactly 1 if all the molecules are sitting on top of a lattice site, while in a disordered system its value is about $1/\sqrt{N}$, where N is the number of particles. The value we find at the equilibrium density is $\langle O \rangle \sim 0.72$ for the molecular degrees of freedom. This value slightly increases with the density of the system as the molecules become more and more localized. At the highest density considered we found $\langle O \rangle \sim 0.76$. The limit of stability for the crystal phase is found at a density $0.0172\text{Å}^{-3} < \rho < 0.0194\text{Å}^{-3}$.

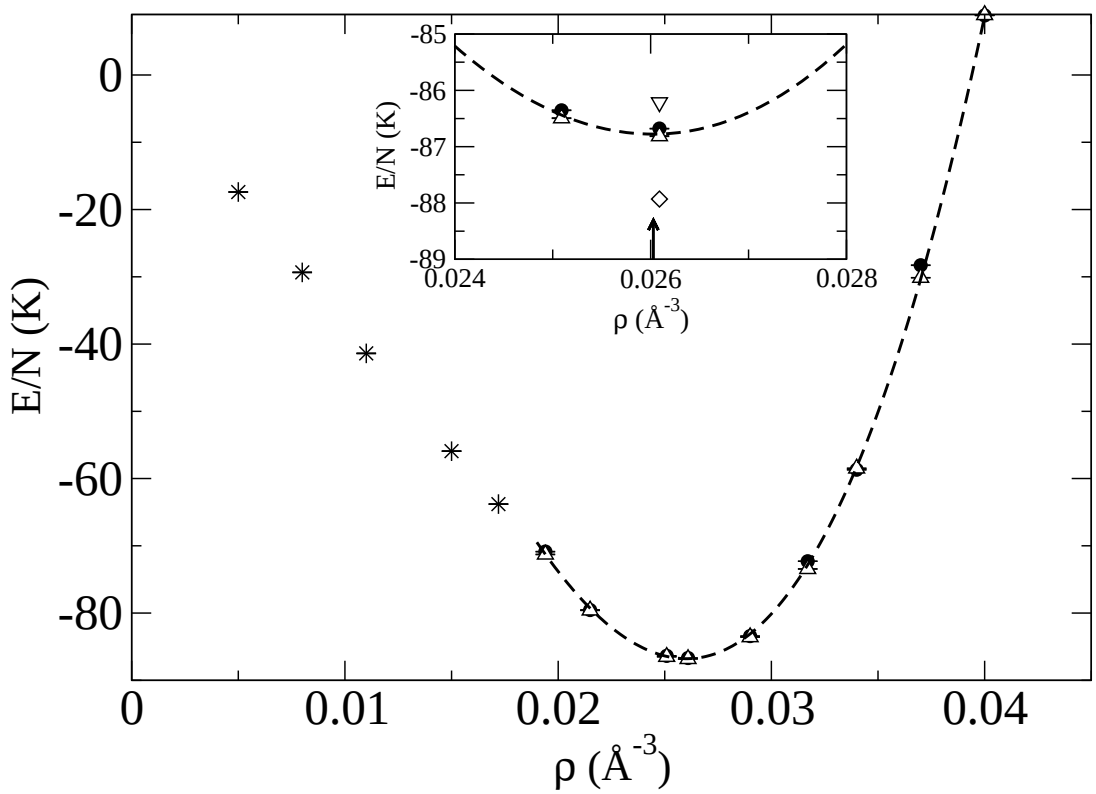


FIG. 2: Estimated energy per molecule in solid and liquid p-H_2 . Filled circles: SWF results for the fcc crystal; empty triangles: SWF results for the hcp crystal; stars: SWF results in the disordered phase. The inset gives an expanded view around the equilibrium density. Filled triangle: JN result; diamond: DMC result. The dashed line is a plot of the fit with Eq. (13). The arrow indicates the equilibrium density obtained by the fit.

In order to compute the value of the equilibrium density and pressure, it is convenient to fit the results for the ground state energy per particle by means of the following expression:

$$E(\rho) = E_0 + a\rho + b\rho^{\gamma}. \tag{13}$$

The coefficients for the solid phase in the fcc and hcp crystals are reported in table V. The estimate of the equilibrium density is in good agreement with the experimental finding $\rho_0^{exp} = 0.02595\text{Å}^{-3}$[2]. The pressure as a function of density is then obtained from the following expression:

$$P(\rho) = \frac{1}{\rho^2}\frac{\partial E(\rho)}{\partial \rho}. \tag{14}$$

In Fig. 3 the computed pressure for the fcc and hcp solid phases is compared to the experimental curve extrapolated to T=0[2]. The SWF result is lower than the experiment

	E_0	a	b	γ	ρ_0 (Å^{-3})
fcc	78.8502	-9205.32	1.02128×10^7	3.24389	0.02601
hcp	82.8656	-9478.60	9.41995×10^6	3.21149	0.02603

T/

en

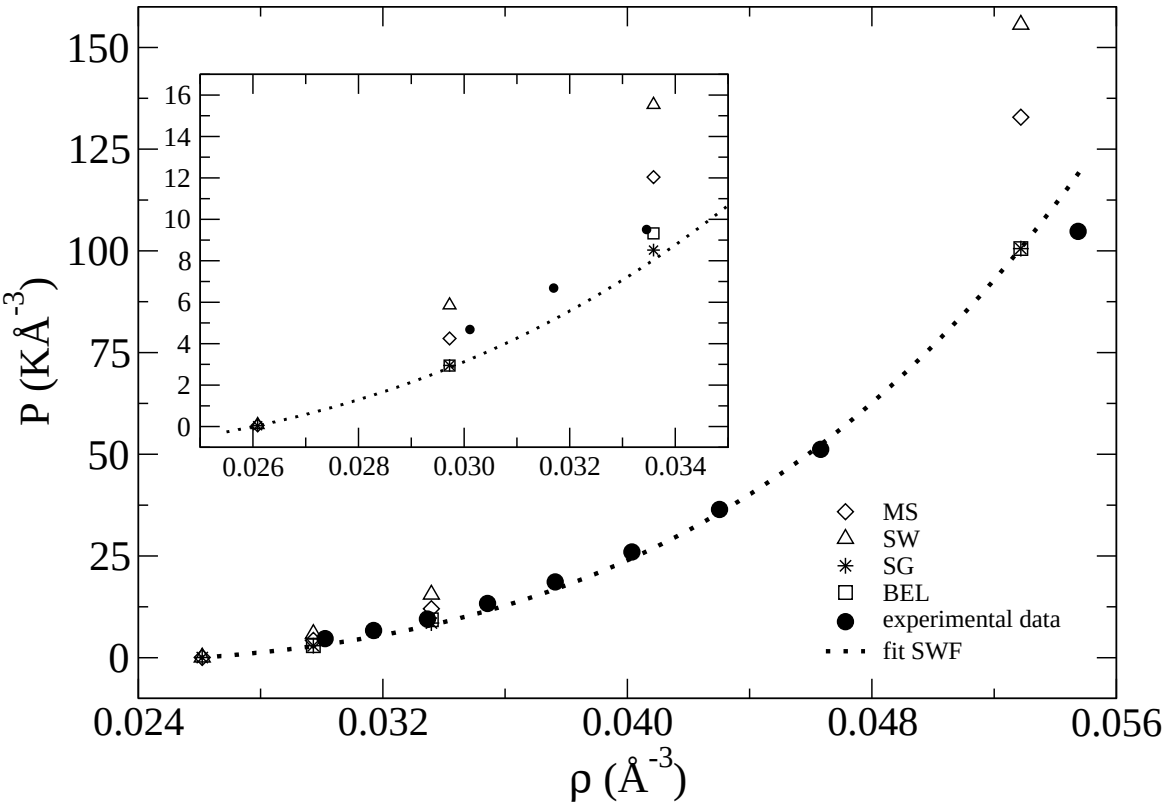


FIG. 3: Pressure as a function of density in solid p-H_2 . Dotted line: SWF result computed from Eq. (15) from the fit of the ground state energy. Filled circles are experimental data from ref. [2]. Points are values computed in ref. [24] with different intermolecular potentials (MS: Meyer and Schaefer[31]; SW: Schaefer and Watts[26]; SG: Silvera and Goldman[23]; BEL: Buck *et al.*[27]). In the inset we expand the same data near the equilibrium density.

near the equilibrium density, while the pressure tends to be overestimated at high densities. We also compare our results with results of Norman et al.[24] for the same Silvera-Goldman potential and for other intermolecular interactions.

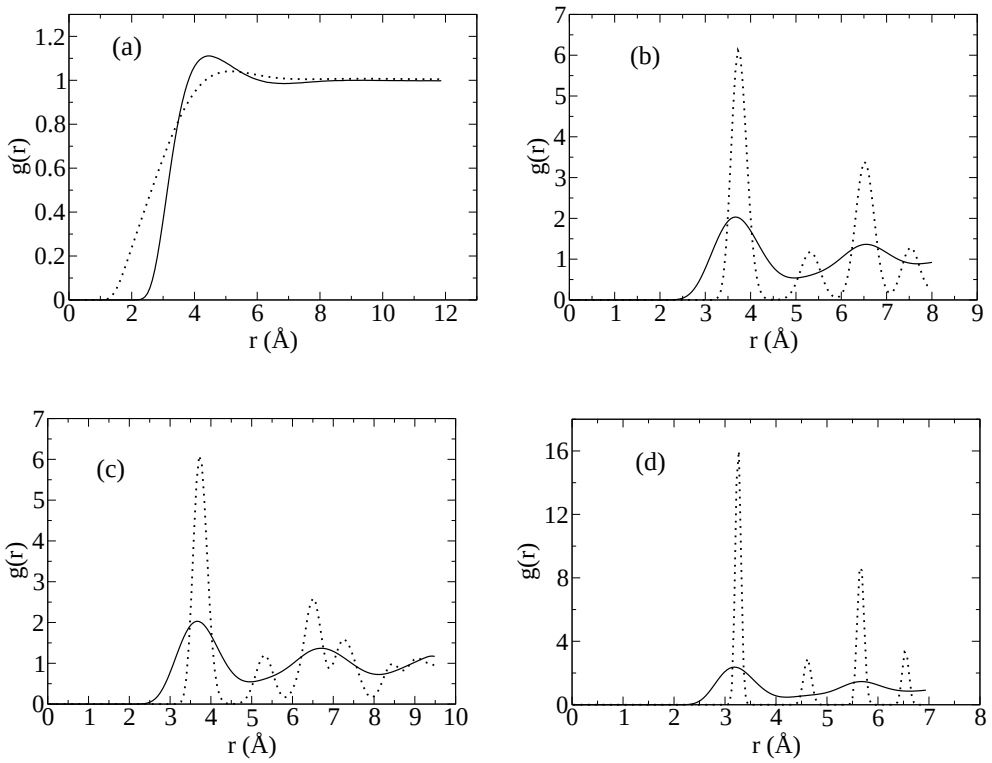


FIG. 4: Pair distribution functions computed with SWF in molecular p-H_2 . Solid lines: pdf of particles; dotted line: pdf for shadows. (a) $\rho = 0.00800\text{Å}^{-3}$ (disordered phase); (b) $\rho = 0.02609\text{Å}^{-3}$ (fcc crystal); (c) $\rho = 0.02609\text{Å}^{-3}$ (hcp crystal); (d) $\rho = 0.04000\text{Å}^{-3}$ (fcc crystal).

In Fig. 4 we plot the pair distribution function:

$$g(r) = \langle \sum_{i \neq j} \delta(|\mathbf{r}_i - \mathbf{r}_j|, r) \rangle, \tag{15}$$

were $\langle\rangle$ indicates the expectation value over the SWF. The same quantity can be defined for the shadow degrees of freedom:

$$g_s(r) = \langle \sum_{i \neq j} \delta(|\mathbf{s}_i - \mathbf{s}_j|, r) \rangle. \tag{16}$$

$g(r)$ and $g_s(r)$ are displayed for a density below ρ_0, at ρ_0 for the fcc and hcp crystals and at an higher density for the fcc crystal. At the lowest density $g(r)$ has the typical behavior that can be observed in a fluid, with a peak at the first shell of about 1.1. At larger densities, where the system is crystallized, it is possible to observe how the first peak increases to values around 2. The peaks corresponding to the second and third shell are nearly merging into each other. This feature, common to other quantum solids, is due to the wide dispersion of the molecules around the lattice sites. On the other hand, the distribution of shadows

presents, as expected, a much better defined structure. The peaks typical of the fcc and hcp structures, already well visible at density ρ_0 become separated at higher densities. The shadow–shadow correlation induces a much stronger localization, and at higher densities the distribution becomes similar to that of a classical solid.

C. Vacancies

The vacancy formation energy at constant pressure in a system of N particles and N_l lattice sites at a given density ρ can be defined as[32, 33]:

$$\Delta E_{vac} = E(V', N = N-1, N_l = N) - \frac{N-1}{N} E(V, N, N_l = N). \tag{17}$$

The volumes V and V' are related by the requirement that the density of the system remains constant, i.e., $N/V = (N-1)/V'$. In a quantum crystal ΔE_{vac} has contributions from three different effects. The main contribution comes from the missing potential and kinetic energy due to the missing particle. At constant pressure and in the thermodynamic limit, this energy is a function of the pressure and of the potential energy per particle:

$$\Delta E^0_{vac} = \frac{1}{\rho} P(\rho) - \frac{V(\rho)}{N}. \tag{18}$$

Another important contribution comes from the relaxation of the crystal around the empty site. This term lowers the vacancy formation energy due to the fact that the kinetic energy of the molecules surrounding the vacancy is reduced. This contribution is more important at lower densities, and can be well described only within a model that allows lattice sites to be displaced from their original positions, as happens for SWF where no *a-priori* lattice is assumed. The third contribution comes from the motion of the vacancy through the crystal. The bandwidth of the vacancy has recently been recently estimated to be 6 to 10K in ^{4}He by Galli and Reatto[34]. We expect this contribution to be smaller in p-H_2 , due to the higher degree of localization of the molecules.

In Fig. 5 we report the results obtained for ΔE_{vac} as a function of the density for the fcc crystal (obtained with N=108 molecules), and for the hcp crystal (obtained with N=180 molecules). The values are compared with the corresponding estimate of ΔE^0_{vac}. As can be seen there is a strong dependence of ΔE_{vac} on the density. For low densities the contribution from lattice relaxation, which can be estimated by the difference $E_{rel} = \Delta E^{vac}_0 - \Delta E^{vac}$, is

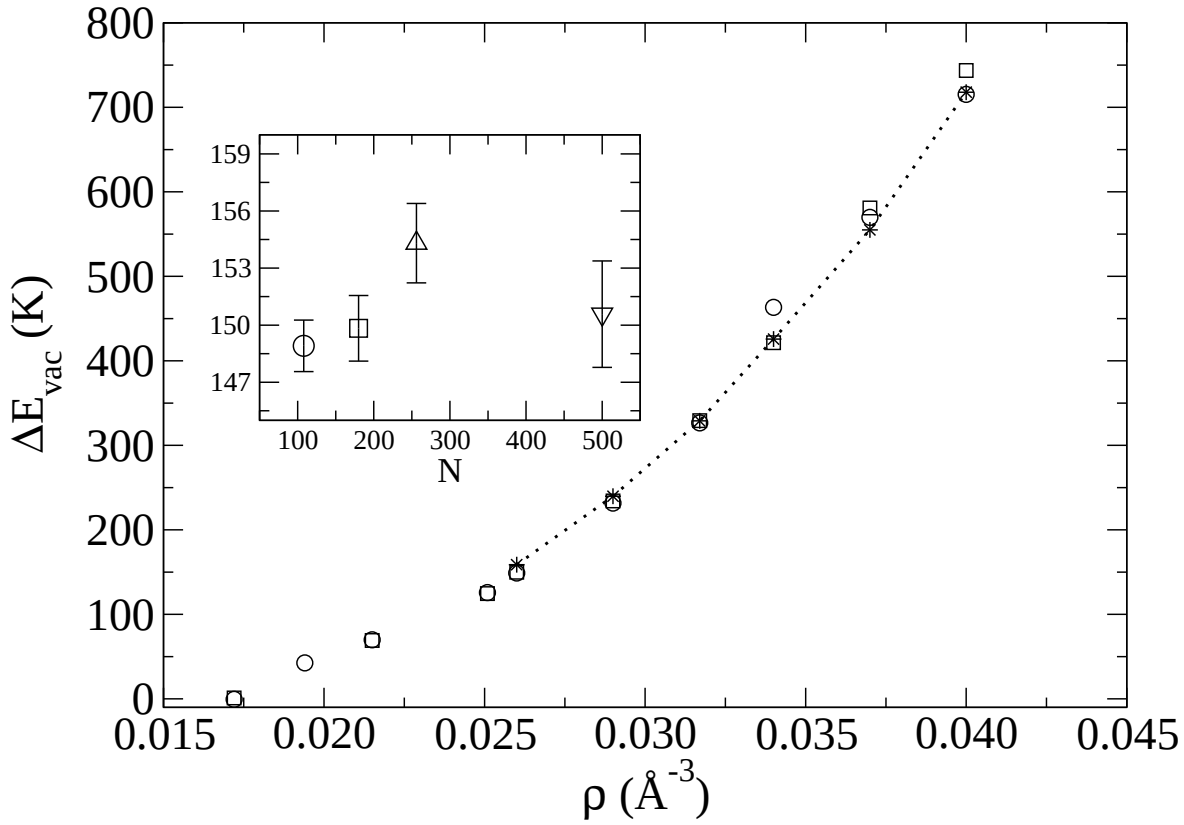


FIG. 5: Vacancy formation energy ΔE_{vac} from SWF calculations as a function of the molecular density. Circles: fcc crystal (108/107 particles); squares: hcp crystal (180/179 particles). The dotted line represents the estimated energy for a vacancy without relaxation effects, obtained from the fitted equation of state. In the inset we plot the vacancy formation energy at density $\rho = 0.02609\text{Å}^{-3}$ as a function of N, the number of particles used in the simulation.

$E_{rel} \sim 9K$. This value decreases when the density increases. For high densities E_{rel} does not show a systematic behavior. The estimate of the energy of a static vacancy depends on the potential energy per particle, which has a larger uncertainty at higher densities due to larger autocorrelations and stronger finite-size effects. Finite size effects also make the estimate of ΔE_{vac} from the variational results harder to obtain. This can also be inferred from the fact that the results for the fcc and hcp lattices tend to depart from each other in a non systematic way. Their difference can be considered as a measure of the actual uncertainty on the computed value of ΔE_{vac} The use of periodic boundary conditions implies that the presence of one vacancy in the simulation cell corresponds to a density 1/N of vacancies in the infinite crystal. The local deformation of the crystal due to the relaxation of the atoms

N	ΔE_{vac} (K)
107	149(1)
179	150(2)
255	154(2)
499	150(3)

TABLE VI: Vacancy formation energy for p-H_2 at density $\rho = 0.02600\text{Å}^{-3}$ as a function of the number of particles used in the simulation.

around the empty site might induce deformations to the next shells, which might translate into a vacancy-vacancy interaction. In order to check if such interaction affects the estimate of the vacancy formation energy, we performed simulations at different numbers of molecules at the equilibrium density (where relaxation effects are large), and recomputed the vacancy formation energy. Results are reported in table VI. As can be seen, the differences are within two standard deviations, suggesting that no sizeable effects of the relaxation can be observed beyond the second shell of neighbors (which is contained in the simulation box with 108 molecules). This is also confirmed by the fact that at density ρ_0 no significant difference is observed for the vacancy formation energy in the fcc and the hcp crystals, that have the same structure for the first shell of neighbors.

IV. CONCLUSIONS

A shadow wavefunction has been devised to study ground state properties of molecular para-hydrogen, using the Silvera–Goldman interaction. The equation of state of the crystalline fcc and hcp phases has been computed optimizing the variational parameters of the SWF, and fitting them as functions of the density. The estimated energy per particle is on average 10% higher than the available experimental data. However the estimate of the pressure and of the equilibrium density suggest that this SWF gives a realistic description of the system, allowing for future developments, in particular for as regards the study of the solid–vapor interface, and the study of clusters. The vacancy formation energy has been estimated in a wide range of densities. At densities around the equilibrium value relaxation effects appear to be about 5% of the total vacancy formation energy.

Acknowledgments

We would like to thank G.V. Chester, M.H. Kalos, S. Fantoni, and L. Reatto for useful comments and suggestions about this work. We also thank C.J. Umrigar for providing us the Levemberg-Marquardt package used for the optimization of the parameters in the Shadow Wave Function. Part of this work was supported by a grant COFIN2002 "Quantum Fluids and Solids in Confined Geometries" of the Italian Ministero dell' Istruzione, Università e Ricerca. Calculations have been performed in part on the Beowulf cluster in CINECA under a INFM parallel computing grant, and in part on the ALPS cluster at ECT* in Trento.

---

[1] R. J. Hemley, H. K. Mao, and J. F. Shu, Phys. Rev. Lett. **65**, 2670 (1990).

[2] J. van Straaten and I. F. Silvera, Phys. Rev. B **37**, 1989 (1988).

[3] I. F. Silvera, Rev. Mod. Phys. **52**, 393 (1980).

[4] I. F. Silvera and R. J. Wijngaarden, Phys. Rev. Lett. **47**, 39 (1981).

[5] H. E. Lorenzana, I. F. Silvera, and K. A. Goettel, Phys. Rev. Lett. **64**, 1939 (1990).

[6] K. J. Runge, M. P. Surh, C. Mailhiot, and E. L. Pollock, Phys. Rev. Lett. **69**, 3527 (1992).

[7] M. P. Surh, K. J. Runge, T. W. Barbee, E. L. Pollock, and C. Mailhiot, Phys. Rev. B **55**, 11330 (1997).

[8] V. L. Ginzburg and A. A. Sobyanin, JETP Lett. **15**, 11330 (1972).

[9] P. Sindzingre, D. M. Ceperley, and M. L. Klein, Phys. Rev. Lett. **67**, 1871 (1991).

[10] A. C. Levi and R. Mazzarello, J. Low. Temp. Phys. **122**, 75 (2001).

[11] M. C. Gordillo and D. M. Ceperley, Phys. Rev. Lett. **79**, 3010 (1997).

[12] K. Nho and E. Manousakis, Phys. Rev. B **65**, 115409 (2002).

[13] M. C. Gordillo and D. M. Ceperley, Phys. Rev. B **65**, 174527 (2002).

[14] M. Wagner and D. M. Ceperley, J. Low Temp. Phys. **102**, 275 (1996).

[15] S. Grebenev, B. Sarkatov, J. P. Toennis, and A. F. Vilesov, Science **289**, 1532 (2000).

[16] Y. Kwon and K. B. Whaley, Phys. Rev. Lett. **89**, 273401 (2002).

[17] S. Vitiello, K. Runge, and M. H. Kalos, Phys. Rev. Lett. **60**, 1970 (1988).

[18] L. Reatto and G. L. Masserini, Phys. Rev. B **38**, 4516 (1988).

[19] F. Pederiva, A. Ferrante, S. Fantoni, and L. Reatto, Phys. Rev. Lett. **72**, 2589 (1994).

[20] D. E. Galli and L. Reatto, J. Low Temp. Phys. **113**, 223 (1998).

[21] D. E. Galli, M. Buzzacchi, and L. Reatto, J. Chem. Phys. **115**, 10239 (2001).

[22] M. V. R. Krishna and K. B. Whaley, Z. Phys. D **20**, 223 (1991).

[23] I. F. Silvera and V. V. Goldman, J. Chem. Phys. **69**, 4209 (1978).

[24] M. J. Norman, R. O. Watts, and U. Buck, J. Chem. Phys. **81**, 3500 (1984).

[25] L. H. Nosanow, Phys. Rev. Lett. **13**, 270 (1964).

[26] J. Schaefer and R. O. Watts, Mol. Phys. **47**, 933 (1982).

[27] U. Buck, F. Huisken, A. Kohlhase, D. Otten, and J. Schaefer, J. Chem. Phys. **78**, 4439 (1983).

[28] T. MacFarland, S. A. Vitiello, L. Reatto, G. V. Chester, and M. H. Kalos, Phys. Rev. B **50**, 13577 (1994).

[29] F. Pederiva, G. V. Chester, S. Fantoni, and L. Reatto, Phys. Rev. B **56**, 5909 (1997).

[30] B. Chaudhuri, F. Pederiva, and G. V. Chester, Phys. Rev. B **60**, 3271 (1999).

[31] J. Schaefer and W. Meyer, J. Chem. Phys. **70**, 344 (1979).

[32] R. A. Guyer, J. Low Temp. Phys. **8**, 427 (1972).

[33] F. Pederiva, F. Dalfovo, S. Fantoni, L. Reatto, and S. Stringari, Phys. Rev. B **55**, 3122 (1997).

[34] D. E. Galli and L. Reatto, Phys. Rev. Lett. **90**, 175301 (2003).